Rev. Adv. Mater. Sci. 31 (2012) 25-30

FINITE ELEMENT ANALYSIS FOR COMPRESSION BEHAVIOR OF HIGH PRESSURE TORSION PROCESSING

Dong Jun Lee[1], Eun Yoo Yoon[1], Sung Hak Lee[1], Soo Young Kang[2] and Hyoung Seop Kim[1]

[1]Department of Materials Science and Engineering, Pohang University of Science and Technology (POSTECH), Pohang, 790-784, Republic of Korea
[2]Dep. of Metallurgical and Material Engineering, Inha Technical College, Incheon 402-752, Republic of Korea

Received: April 20, 2012

Abstract. In this study, plastic deformation behavior of commercially pure copper, during a compression stage of the high pressure torsion (HPT) process, was employed using the finite element method. Numerical simulations dealt with a phenomenological constitutive model based on dislocation density evolutions. After the compression, the effective strains reached locally over 2 and the effective stress was approximately 500 MPa. These stress and strain values during the compression are sufficiently high for grain refinement by severe plastic deformation and for hardening of the material. The compression stage should be considered for the theoretical as well as experimental analyses of the HPT process.

1. INTRODUCTION

Recently, severe plastic deformation (SPD) processing has been developed as a "top-down" approach to manufacture bulk metallic materials with ultrafine grain (UFG) and nanostructure which have improved mechanical and physical properties [1-8]. Among various SPD processes, high pressure torsion (HPT) is the most effective process for grain refinement since extraordinarily large strain can be imposed on the work piece much easily compared to any other SPD processes, such as the well-known equal channel angular pressing [9-12], heavy rolling [13,14], and friction stir welding [15-17] processes.

The concept of HPT was first proposed over 70 years ago [18], while it has been investigated again for grain refinement in the present decade [19,20]. The HPT process consists of two stages as shown in Fig. 1: the first stage is compression using high pressure of the dies and the second is torsion maintaining the die pressure. A large amount of shear deformation is imposed on the disk-shaped sample by the multiple rotations of the die during the torsional process; hence most of the previous studies were focused on the microstructures and mechanical properties after the second(torsion) stage. However, according to the recent report of Song *et al*. [21], the compression stage is also important in the whole HPT processing and a large amount of plastic deformation (of course, less than that in the torsion stage) is already developed during the compression stage as well. In order to understand the HPT process, theoretical analyses as well as experimental approaches of the process are necessary. Several papers [22-25] were reported for the theoretical analysis of HPT processing using the finite element method (FEM).However, there have been no reports on plastic deformation analysis during the compressive stage of HPT, as far as the authors know. In addition, for more informative simulations of the HPT processing, we need a constitutive model to describe the large strain deformation of polycrystalline materials.

In this study, plastic deformation behavior of the workpiece during the compression stage in the HPT process is investigated by using the FEM combined

Corresponding author: Hyoung Seop Kim, e-mail: hskim@postech.ac.kr

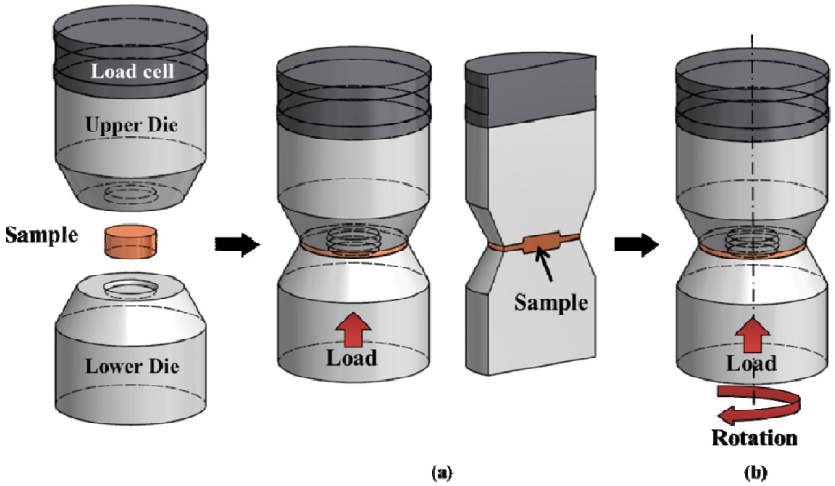

Fig. 1. Schematic of the HPT device showing the set-up: (a) compression stage and (b) compression-torsion stage.

with a microstructure based constitutive model. In order to describe the large strain deformation of polycrystalline materials, a constitutive model associated tothe evolution of dislocation density with one internal variable [26] is applied. The simulation results are discussed and verified with experimental results by Song *et al*. [21].

2. DISLOCATION BASED UNIFIED CONSTITUTIVE MODEL [26]

The constitutive model employed in this paper starts from an assumption that the material is plastically isotropic even under large plastic deformation. Total strain rate is given by the sum of the elastic strain rate and the plastic strain rate. The elastic strain rate is given by the Hooke's law, while the plastic strain rate $\dot{\varepsilon}^{p}_{c,u}$ is expressed in the form of the Lévy-von Mises equation, Eq. (1).

$$\dot{\varepsilon}^{p}_{c,u} = \dot{\varepsilon}_{*}\left(\sigma/\sigma_{0}\right)^{m}, \tag{1}$$

where σ is stress, the quantity σ_0 is an initial stress related to the initial dislocation density, the stress exponent *m* is inversely proportional to temperature and the constant $\dot{\varepsilon}_{*}$ is a strain normalization factor.

The evolution of dislocation density in the process of plastic deformation is described by

$$\mathrm{d}Z/\mathrm{d}\varepsilon^{p}_{c,u} = C + C_1\sqrt{Z} - C_2 Z \tag{2}$$

[26], where *Z* is a dislocation density normalized by its initial value. In Eq. (2), the coefficients *C* and C_1 indicate strain hardening by dislocation storage, and C_2 indicates recovery due to dislocation annihilation. The mechanism of the dislocation storage is not dependent on temperature, hence C_1 becomes a constant. On the contrary, as temperature increases, recovery by dislocation cross-slip or dislocation climb, takes place more. Therefore, C_2 can be expressed as follows:

$$C_2 = C_{20}\left(\frac{\dot{\varepsilon}^{p}_{c,u}}{\dot{\varepsilon}_{0}}\right)^{-1/n}, \tag{3}$$

where C_{20} and $\dot{\varepsilon}_{0}$ are constants and the exponent *n* is a constant inversely proportional to temperature. Considering coarse-grained materials, *C* in Eq. (2) can be zero. For fine-grained materials, however, it is inversely proportional to grain size *d*.

$$C = M\frac{b}{d}\left(\frac{M\alpha G}{\sigma_{0}}\right)^{2}, \tag{4}$$

where *M* is the Taylor factor, *b* is the magnitude of the dislocation Burgers vector, *G* is the shear modulus, and a is a numerical constant.

The tensile testing was conducted with a strain rate of 1.0×10^{-3} s^{-1} for commercial purity copper (99.98%) annealed at 873K for 2 h. The stress-strain curve was obtained as shown in Fig. 2. From the tensile testing results and Ref. [26], the parameters in the above constitutive model are determined for the best fitted stress-strain curve as can be seen in Fig. 2.

3. FINITE ELEMENT ANALYSIS

The isothermal finite element simulations for the compression stage in HPT have been carried out using the commercial rigid-plastic finite element code, DEFORM-2D ver. 9.1 [27]. The user defined

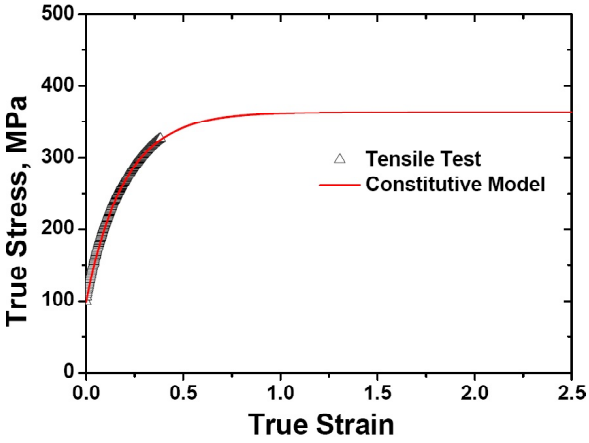

Fig. 2. Flow stress-strain curves of commercial pure copper obtained by constitutive equation (line) and tensile testing (symbol).

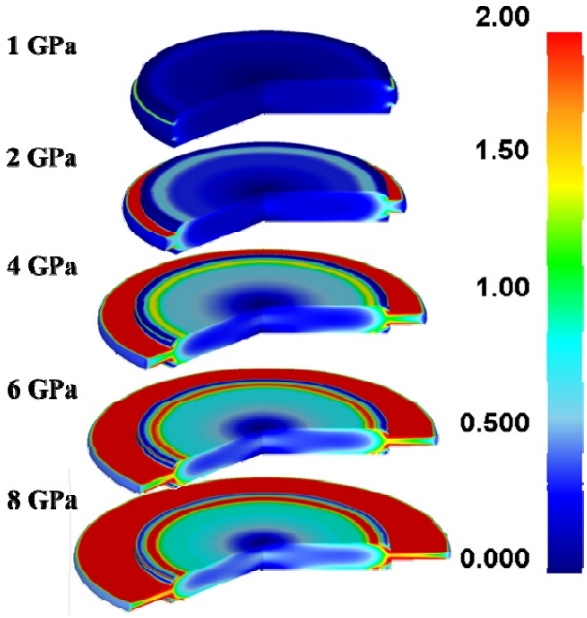

Fig. 3. Effective strain distributions from the results of the finite element analysis after the compression stages of HPT.

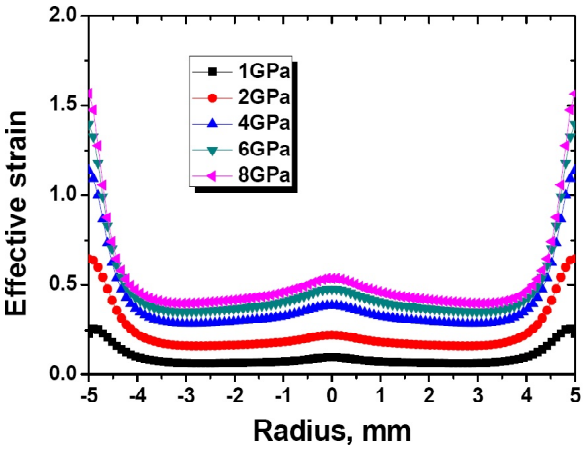

Fig. 4. Path plots of the effective strain along a radial direction on the mid-plane from the results of finite element analysis after the compression stage of HPT.

subroutine in the DEFORM-2D software was applied to present simulations using the abovementioned dislocation density-based constitutive model. The axisymmetric condition was used in geometry of the workpiece: the initial dimensions of the workpiece were 5 mm in radius and 1.5 mm in thickness. The number of elements in the workpiece was 10,000, which was enough to show the local deformation behavior. The upper and lower dies are 10 mm in diameter and 2.5 mm in thickness of depression. In the compression stage, the speed of the top die was 0.1 mm/s until a pressure of 8 GPa was imposed on the workpiece. The friction factor between the die and the workpiece during the compression was set to be as 1.0, which is a proper value since the roughness of the surface of the dies is high enough to prevent slippage between the workpiece and the die.

4. RESULTS AND DISCUSSION

Fig. 3 shows effective strain distributions and deformed geometries of the sample in the HPT die under various applied pressure values of 1, 2, 4, 6, and 8 GPa. The deformed shape of the 1 GPa sample is still similar to the initial flat disk, while the samples 2 GPa exhibit step and flash, with material forced outward from the workpiece. The flash expands as the imposed pressure increases. The role of the flash is to constrain free expansion of the workpiece. Hence controlling flash is crucial for successful metal forming because it determines forming loads and the deformed shapes of the workpiece: small flash induces incomplete die filling and large flash generates redundant load [21]. Without a constraint by the edge flash, the workpiece in the open die will become thin and flat under high pressures of several GPa. Growth of the edge flash with applied pressure implies that the thickness of the workpiece decreases.

The effective strain increases and the flash region (outside of the inner die blank) expands as the applied pressure increases. The path plots of the effective strain along aradial direction on the mid-plane for each applied pressure were presented in Fig. 4. The effective strain increases up to 0.07-0.25 after 1 GPa and up to 0.40-1.56 after 8 GPa. The effective strain at the edge is the highest, while in the middle region of the disk, *i.e*. 3 mm from the

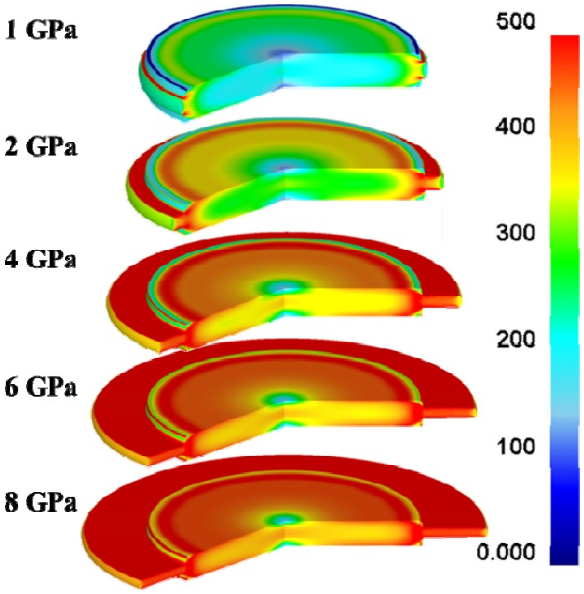

Fig. 5. Effective stress distributions from the results of finite element analysis after the compression stage of HPT.

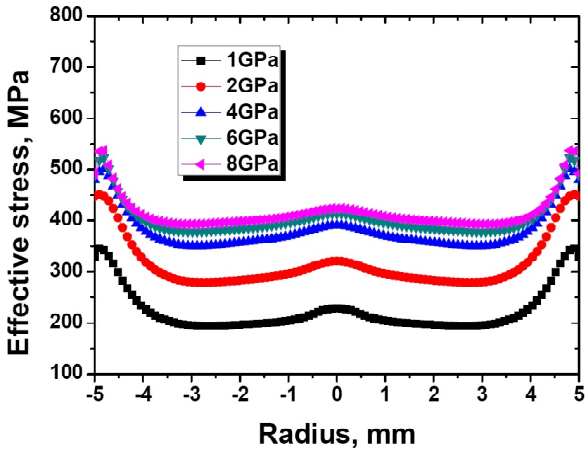

Fig. 6. Path plots of the effective stress along a radial direction on the mid-plane from the results of finite element analysis after the compression stage of HPT.

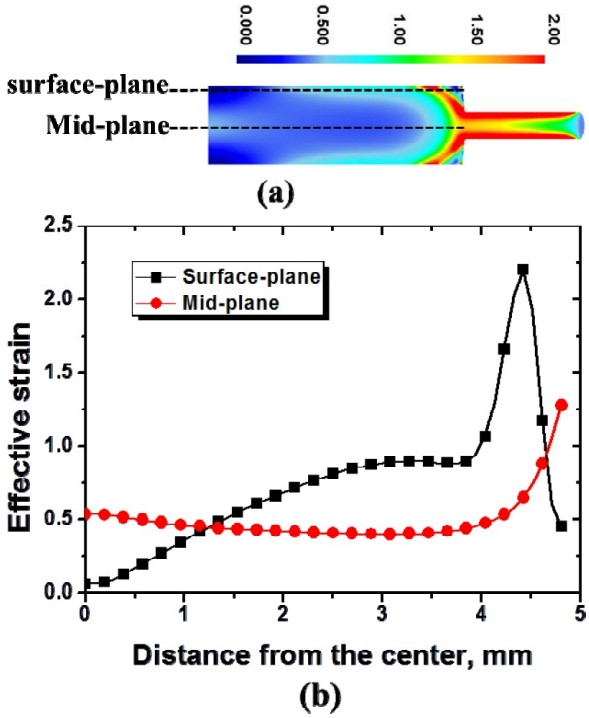

Fig. 7. (a) Positions for effective strain distributions after 8 GPa compression and (b) path plots of the effective strain on the surface and mid-planes indicated in (a).

center, strain is smaller than that in the center region.

This tendency of the lowest deformation in the middle region is also shown in the effective stress distributions along the mid-plane in Figs. 5 and 6. These are due tothe flash and the frictional stress between dies and workpiece. In the quasi-constrained condition [3], the flash is formed by high pressure between the dies. Hence, the flash expands as the applied pressure increases and material flows outward. Furthermore, the lateral vertical wall of the die prevents the flow of the material. Therefore, the flash and the vertical wall produce high plastic deformation in the edge of the workpiece. The friction between the dies and material causes the 'friction hill' at the center of the die contacting surface, meaning that a higher compressive stress is generated near the center of the disk [21,28,29]. If there is no friction between the material and the dies, the normal pressure on the material would be constant. However, high friction force due to the high friction and high compressive stress in HPT process retards the outward flow of the material. The compressive stress, by the friction hill is high at the center. Therefore, the effective strain and stress in the center regions are higher than those in the middle. This phenomenon is also found in the study of the hardness distributions by Song *et al*. [21]. According to the hardness distributions, the center on the mid-plane increased up to 120 HV under pressure of 8 GPa, whereas middle region was 110 HV. It can be found that the hardness at the center is higher than middle region of specimen during compression.

Fig. 7 shows cross-sectional strain distributions on the surface-plane and mid-plane after compression under pressure of 8 GPa. It clearly exhibits strain in homogeneity during compression stage in Fig. 7a. As mentioned in the previous paragraph, on the mid-plane, the effective strain in the center region is higher than in the middle region and the

highest strain region is the edge region due to the effects of the flash and the friction hill. On the surface plane, however, the effective stain presents completely different result (Fig. 7b). The effective strain is the lowest in the center of the sample and increases along the radial direction due to the high friction and die design. The high friction prevents radial expansion of the material during the compression and creates a low strained zone in the center of sample at the top and bottom surfaces. This is a well-known phenomenon in compression tests [29]. Moreover, the effective strain on the surface-plane increases from center to edge due to the friction.

After the compression, the strain and stress values are significantly high because of the heavy plastic deformation and hardening behavior of material.The local strain and stress values reach almost 2 and 500 MPa, respectively. The saturated hardness of copper after HPT process reaches140 Hv noted by several papers [30, 31]. From the hardness results [21], after 8 GPa of pressure, the hardness increases up to 120 Hv from the initial value of 55 Hv. The large amount of hardening is generated during the compression stage.

5. CONCLUSIONS

In this paper, we investigated the compression stage in the HPT processing using the finite element method. The effective strain increased up to 1.56 after 8 GPa. The effective strain and stress in the center region on the mid-plane were larger than those in the middle region due to the flash and the friction hill. In contrast, on the surface plane, the effective strain in the center was lower than that in the middle region due to the high friction between die and workpiece. After the compression, the strain and stress values are significantly increased by the plastic deformation and hardening behavior of material. Therefore, the compression stage in the HPT process is important and should not be ignored, especially the analysis of the early hardening behavior by torsional process in HPT.

ACKNOWLEDGEMENT

This study was supported by a grant from the Fundamental R&D Program for Core Technology of Materials (100372751-55551) funded by the Ministry of Knowledge Economy, Korea.

REFERENCES

[1] R.Z. Valiev, R.K. Islamgaliev and I.V. Alexandrov // *Prog. Mater. Sci*. **45** (2000) 103.
[2] M.A. Meyers, A. Mishra and D.J. Benson // *Prog. Mater. Sci*. **51** (2006) 427.
[3] A.P. Zhilyaev and T.G. Langdon // *Prog. Mater. Sci*. **53** (2008) 893.
[4] Y.G. Ko, B.U. Lee and D.H. Shin // *J. Korean Inst. Met. Mater*. **49** (2011) 291.
[5] M. Vaseghi, A.K. Taheri and H.S. Kim // *Met. Mater. Int*. **16** (2010) 363.
[6] G. Purcek, O. Saray and O. Kul // *Met. Mater. Int.* **16** (2010) 145.
[7] K.H. Song, H.S. Kim and W.Y. Kim // *J. Korean Inst. Met. Mater*. **49** (2011) 649.
[8] S.J. Yoo and W.J. Kim // *J. Korean Inst. Met. Mater*. **49** (2011) 104.
[9] M.I. Abd El Aal, N. El Mahallawy, F.A. Shehata, M.A. El Hameed, E.Y. Yoon, J.H. Lee and H.S. Kim // *Met. Mater. Int.* **16** (2010) 709.
[10] K.J. Cho and S.I. Hong // *J. Korean Inst. Met. Mater*. **49** (2011) 128.
[11] J.H. Ji, L.J. Park, H.W. Kim, S.W. Hwang, C.S. Lee and K.T. Park // *J. Korean Inst. Met. Mater*. **49** (2011) 474.
[12] Y-G. Jin, I-H. Son and Y-T. Im // *Met. Mater. Int*. **16** (2010) 413.
[13] S-H. Lee and C-S. Kang // *J. Korean Inst. Met. Mater*. **49** (2011) 893.
[14] J.M. Kim, J.S. Park and K.T. Kim // *Met. Mater. Int*. **16** (2010) 657.
[15] D. Kim, H. Badarinarayan, I. Ryu, J.H. Kim, C. Kim, K. Okamoto, R.H. Wagoner and K. Chung // *Met. Mater. Int.* **16** (2010) 323.
[16] J. Kim, W. Lee, K.H. Chung, D. Kim, C. Kim, K. Okamoto, R.H. Wagoner and K. Chung // *Met. Mater. Int.* **17** (2011) 83.
[17] N.K. Kim, B.C. Kim, B.H. Jung, S.W. Song, K. Nakata and C.Y. Kang // *J. Korean Inst. Met. Mater.* **48** (2010) 533.
[18] P.W. Bridgman // *J. Appl. Phys*. **14** (1943) 273.
[19] A.P. Zhilyaev, G.V. Nurislamova, B.K. Kim, M.D. Baró, J.A. Szpunar and T.G. Langdon // *Acta Mater*. **51** (2003) 753.
[20] T. Hebesberger, H.P. Stüwe, A. Vorhauer, F. Wetscher and R. Pippan // *Acta Mater.* **53** (2005) 393.
[21] Y. Song, E.Y. Yoon, D.J. Lee, J.H. Lee and H.S. Kim // *Mater. Sci. Eng. A***528** (2011) 4840.
[22] H.S. Kim // *J. Mater. Process. Technol*. **113** (2001) 617.
[23] H.S. Kim, S.I. Hong, Y.S. Lee, A.A. Dubravina and I.V. Alexandrov // *J. Mater. Process. Technol.* **142** (2003) 334.

[24] S.C. Yoon, Z. Horita and H.S. Kim // *J. Mater. Process. Technol*. **201** (2008) 32.
[25] R.B. Figueiredo, P.R. Cetlin and T.G. Langdon // *Mater. Sci. Eng. A***528** (2011) 8198.
[26] Y. Estrin, In: *Unified Constitutive Laws of Plastic Deformation*, ed. by: A.S. Krausz and K. Krausz (New York, 1995), p. 69.
[27] *DEFORM software, in Scientific Forming Technologies Corp., Columbus*.
[28] G.E. Dieter, *Mechanical metallurgy* (McGraw-Hill, 1976).
[29] W.F. Hosford and R. Caddell, *Metal Forming: Mechanics and Metallurgy* (Cambridge University Press, 2011).
[30] X.H. An, S.D. Wu, Z.F. Zhang, R.B. Figueiredo, N. Gao and T.G. Langdon // *Scripta Mater*. **63** (2010) 560.
[31] Z. Horita and T.G. Langdon // *Mater. Sci. Eng. A***410-411** (2005) 422.